

DualFocus: A Unified Framework for Integrating Positive and Negative Descriptors in Text-based Person Retrieval

Yuchuan Deng
Sichuan University
Chengdu, China
dengyuchuan@stu.scu.edu.cn

Zhanpeng Hu
Sichuan University
Chengdu, China
lucas@stu.scu.edu.cn

Jiakun Han
Sichuan University
Chengdu, China
hjackey9797@gmail.com

Chuang Deng
Sichuan University
Chengdu, China
dengchuang@stu.scu.edu.cn

Qijun Zhao
Sichuan University
Chengdu, China
qjzhao@scu.edu.cn

ABSTRACT

Text-based person retrieval (TPR) aims to retrieve images of a person from an extensive array of candidates based on a given textual description. The core challenge lies in mapping visual and textual data into a unified latent space. While existing TPR methods concentrate on recognizing explicit and positive characteristics, they often neglect the critical influence of negative descriptors, resulting in potential false positives that fulfill positive criteria but could be excluded by negative descriptors. To alleviate these issues, we introduce DualFocus, a unified framework for integrating positive and negative descriptors to enhance the interpretative accuracy of vision-language foundational models regarding textual queries. DualFocus employs Dual (Positive/Negative) Attribute Prompt Learning (DAPL), which integrates Dual Image-Attribute Contrastive (DIAC) Learning and Sensitive Image-Attributes Matching (SIAM) Learning. This way DualFocus enhances the detection of unseen attributes, thereby boosting retrieval precision. To further achieve a balance between coarse and fine-grained alignment of visual and textual embeddings, we propose the Dynamic Tokenwise Similarity (DTS) loss, which refines the representation of both matching and non-matching descriptions, thereby enhancing the matching process through a detailed and adaptable similarity assessment. By focusing on token-level comparisons, DualFocus significantly outperforms existing techniques in both precision and robustness. The experiment results highlight DualFocus’s superior performance on CUHK-PEDES, ICFG-PEDES, and RSTPReid.

CCS CONCEPTS

• **Text-based Person Retrieval, Cross-modal Alignment;**

KEYWORDS

Text-based Person Retrieval, Cross-modal Alignment

1 INTRODUCTION

Text-based Person Retrieval (TPR) [17] is a task at the intersection of multimedia and multimodal retrieval, aiming to identify the most closely matching target pedestrian image from a query text. This technology finds application across a broad spectrum of domains, including social media analytics, image retrieval, and security surveillance. Central to TPR is the challenge of navigating through extensive visual databases to locate images of individuals



Figure 1: Illustration of the effect of negative descriptors. The green box signifies a triumphant retrieval, whereas the red box delineates a failed retrieval. Negative descriptors play a crucial role by providing extra information that narrows down the search parameters, allowing for a more precise identification of an individual.

described by textual cues, necessitating a sophisticated amalgamation of visual and textual information.

In recent advancements, prior works [1, 9, 13, 18, 28, 29, 33], have been achieved in enhancing the precision and efficiency of image searches and person recognition, leveraging the capabilities of Vision-Language Foundation Models (VLFM) such as CLIP [20] and ALIGN [16]. Traditionally, as illustrated in Figure 1, TPR approaches have primarily concentrated on harnessing explicit, positively defined characteristics, like ‘wearing a grey jacket’. This focus often overlooks negative descriptors—attributes identified as absent. This oversight, for example, ignoring phrases like ‘not wearing glasses’, allows the system to keep candidates that meet positive criteria but overlooks filtering out those that should be excluded based on negative descriptors. We suggest that the inadequate management of negative descriptions in TPR may arise from the inherent difficulties VLFM faces in handling fine-grained tasks like attribute detection [30].

To address the identified challenge effectively, we introduce DualFocus: an innovative and comprehensive framework specifically

crafted to highlight the paramount importance of incorporating both positive and negative descriptors. Central to our framework is the development of a Dual Attribute Prompt Learning (DAPL) mechanism. This mechanism is enriched by two novel components: Dual Image-Attribute Contrastive Learning and Sensitive Attributes Prompt Matching Learning. Together, these components are ingeniously designed to amplify the detection capabilities for previously unseen attributes, while ensuring a meticulous alignment between textual descriptions and corresponding image patch embeddings. Further augmenting our framework's efficacy, we unveil the Dynamic Tokenwise Similarity (DTS) loss. This innovative loss function is a cornerstone in our strategy, aimed at refining and improving the congruence between textual narratives and visual representations. By employing DTS loss, DualFocus makes significant strides towards achieving a more nuanced and precise alignment of textual descriptions with their visual counterparts, thereby setting a new benchmark in the domain of text-based person retrieval. This groundbreaking strategy meticulously aligns matching and mismatching descriptions at the token level, offering a nuanced and dynamic evaluation of similarity. Our findings demonstrate that by aligning fine-grained attributes in a unified embedding space and employing a balanced positive-negative granularity loss, we significantly enhance the DualFocus model's performance in accurately matching complex attributes.

Our contributions can be summarized as follows:

- **Dual Attribute Prompt Learning (DAPL) Approach:** Our innovative approach harnesses both positive and negative descriptors to enhance the detection of previously unseen attributes. We incorporate Dual Image-Attribute Contrastive (DIAC) Learning and Sensitive Image-Attributes Matching (SIAM) Learning to achieve precision in aligning textual descriptions with corresponding image patches. This strategy markedly differentiates our work from traditional attribute recognition techniques, providing a more nuanced and accurate framework for attribute detection.
- **DualFocus Framework:** Building on the DAPL Approach, the DualFocus framework enhances CLIP's ability to interpret complex textual prompts through a sophisticated fine-tuning protocol. It intricately balances the consideration of positive and negative descriptors, fostering a nuanced understanding of textual queries and elevating the standard for text-based person search.
- **Dynamic Tokenwise Similarity (DTS) Loss:** Departing from traditional loss functions, the DTS Loss introduces a token-level similarity assessment. This dynamic evaluation mechanism fine-tunes the model's sensitivity to attribute complexity and descriptive depth, significantly improving the alignment of attributes and the interpretation of subtle nuances across a wide spectrum.

2 RELATED WORK

2.1 Text-to-image Person Retrieval

The landscape of Text-based Person Retrieval (TPR) has dramatically evolved, shifting from its initial emphasis on global feature extraction towards a sophisticated paradigm that accentuates local feature alignment and the incorporation of auxiliary tasks. In

the domain of global matching, strategies [3, 10, 13, 24] have been developed to master a comprehensive similarity metric between images and textual descriptions, aiming to foster improved alignment, which collectively advocate for a unified understanding across diverse content types. The emergence of local matching techniques, including contributions from [5, 22, 24, 25, 28], represents a pivotal advancement. These methods, by focusing on the alignment of local attributes, address the shortcomings of global matching, delivering heightened accuracy albeit at the cost of increased computational requirements. Furthermore, the pursuit of auxiliary tasks as a mechanism for implicit alignment opens new avenues for research. Studies such as [1, 9, 13, 19, 23, 27], leverage vision-language pretraining models to forge superior representations, marking a strategic pivot towards the integrated utilization of different learning paradigms. A particularly innovative stride is made by [29], which posits the concept of attribute prompt learning. This approach capitalizes on attribute prompts for meticulous image-attribute alignment, concurrently bolstering text matching learning. Such reciprocal enhancement between text matching and attribute prompt learning enables a deeper engagement with fine-grained details. Shifting from traditional methods focused on feature alignment or auxiliary tasks, our innovative strategy employs dual attribute prompt learning. This approach, integrating both positive and negative descriptors, allows for a nuanced interpretation of textual queries.

2.2 Vision-Language Pre-training

Recent advancements in Vision-Language Pretrained Models (VLP) have harnessed vast datasets of image-text pairs to explore complex semantic interplays between visual and textual data. Central to these innovations is the "pre-training and fine-tuning" paradigm [2, 4, 11]. Through this paradigm, models are meticulously refined across a spectrum of tasks, including image-text contrastive learning [16, 20, 32], masked language modeling [15, 30, 32], and image caption generation [6, 15]. The result is the generation of contextually nuanced and semantically rich representations. These refined representations foster a deeper integration of visual and textual elements, markedly enhancing the efficacy of VLP models in downstream tasks.

3 METHOD

3.1 DualFocus Architecture

3.1.1 The Architecture Overview. Figure 2 outlines our DualFocus framework. This framework is built with five encoders: one Image Encoder (E_I), three Text Encoders (E_T) with consistent weights, and two Cross Encoders (E_C) [13]. To elucidate the components of our model, we define our training dataset as $D = \{I_i, T_i\}_{i=1}^N$, comprising N image-text pairs, where I_i is an image of a person and T_i its textual description. Following [29], we perform text analysis on each T_i to extract and map attributes A_i from a predefined attribute set \mathcal{A} . This mapping generates positive prompts A_i^p for detected attributes and negative prompts A_i^n for absent ones. These prompts serve as inputs for our image-attribute streams, which calculate similarity scores between the image embeddings and both positive and negative attribute prompts, enhancing attribute detection accuracy. Further details on these processes are provided in the following sections.

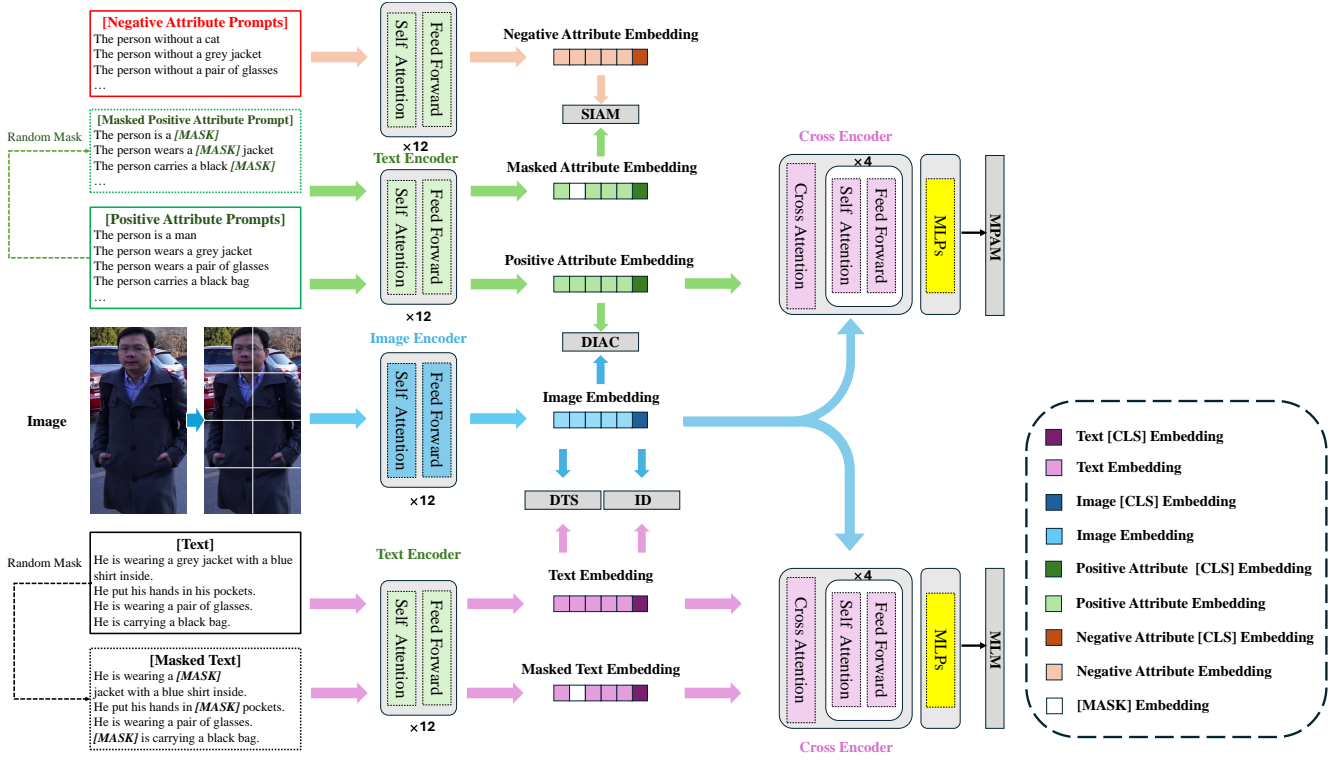


Figure 2: Overview of the proposed DualFocus framework. It consists of five encoders: one Image Encoder (E_I), three Text Encoders (E_T), and two Cross Encoders (E_C). The Image Encoder generates embeddings from visual inputs, while the Text Encoders produce embeddings from textual data. The Cross Encoders integrate these embeddings to enhance cross-modal prediction tasks. Text in grey boxes indicates tasks related to learning processes. Training strategies include Dual Image-Attribute Contrastive Learning (DIAC), which distinguishes images based on attributes; Sensitive Image-Attributes Matching Learning (SIAM), aligning attributes in text with images; Dynamic Tokenwise Similarity Loss (DTS), adjusting token similarity measures for accuracy; Masked Positive Attribute Language Modeling (MPAM), predicting masked positive attributes in context; and Masked Language Modeling (MLM), improving understanding by predicting missing words in sentences. Identity loss (ID), which ensures the preservation and recognition of individual characteristics across different modalities.

3.1.2 Visual Representation Extraction. Given an input image I_i , we initially divide it into a series of equally-sized, non-overlapping patches. These patches are then fed into an image encoder E_I , producing a set of high-dimensional embeddings $\{v_k^i\}_{k=1,2,\dots,n_v}$. To capture the global features of the entire image, a learnable v_{cls}^i token is incorporated. Consequently, the final visual representations are formulated as $F_I^i = \{v_{cls}^i, v_1^i, v_2^i, \dots, v_{n_v}^i\}$.

3.1.3 Textual Representation Extraction. For the input text T_i , we employ a Text Encoder E_T to map the textual information into a corresponding high-dimensional embedding space. Specifically, we process the text through lower-case byte pair encoding (BPE) [21] with a vocabulary size of 49,152. The resultant sequence of textual tokens is augmented with [SOS] and [EOS] tokens to denote the beginning and end of the sequence, respectively. Consequently, the final textual representations are formulated as $F_T^i = \{t_{sos}^i, t_1^i, t_2^i, \dots, t_{n_t}^i, t_{eos}^i\}$. Similarly, attribute prompts are embedded as F_{AP}^i for positive prompts and F_{AN}^i for negative prompts.

3.2 Dynamic Tokenwise Similarity Loss

CLIP's [20] reliance on global representations limits attribute precision within images. To address this, we combine token-level similarity computations [30] with SDM [13] loss to form the Dynamic Tokenwise Similarity (DTS) loss, enhancing fine-grained correspondences between image and text.

Given a batch of image features and text features $\{(F_I^i, F_T^j), y_{i,j}\}_{j=1}^B$, where B is the batch size and $y_{i,j}$ is a binary label indicating whether the pair (F_I^i, F_T^j) shares the same identity ($y_{i,j} = 1$ for a match, and $y_{i,j} = 0$ otherwise). For each visual token in F_I^i , we compute its similarity with all tokens in F_T^j , selecting the highest as the token-wise maximum similarity $\xi_{i,j}^I$, for each image-text pair as follows:

$$\xi_{i,j}^I(F_I^i, F_T^j) = \frac{1}{n_v} \sum_{k=1}^{n_v} \text{sim}(v_k^i, t_{m_k^j}^j), \quad (1)$$

where $\text{sim}(\cdot)$ denotes the cosine similarity function. The index m_k^j , which corresponds to the maximal similarity for each visual token,

is determined by:

$$m_k^I = \arg \max_{0 \leq r < n_r^I} \text{sim}(\mathbf{v}_k^I, \mathbf{t}_r^I). \quad (2)$$

This token-level comparison allows for capturing and contrasting features with greater detail. Non-padded tokens from image and text samples are represented as \mathbf{F}_I^i and \mathbf{F}_T^j , respectively.

The probability of image-to-text matching $p_{i,j}^{i2t}$ is evaluated using a softmax function, defined as:

$$p_{i,j}^{i2t}(\mathbf{F}_I^i, \mathbf{F}_T^j) = \frac{\exp\left(\frac{\xi_{i,j}^I(\mathbf{F}_I^i, \mathbf{F}_T^j)/\tau}{\sum_{k=1}^B \exp\left(\frac{\xi_{i,k}^I(\mathbf{F}_I^i, \mathbf{F}_T^k)/\tau}{\tau}\right)}\right)}{\sum_{k=1}^B \exp\left(\frac{\xi_{i,k}^I(\mathbf{F}_I^i, \mathbf{F}_T^k)/\tau}{\tau}\right)}, \quad (3)$$

where τ is a temperature hyperparameter which controls the probability distribution peaks. Then the DTS loss from images to text in a mini-batch is computed by:

$$\mathcal{L}_{i2t} = \frac{1}{B} \sum_{i=1}^B \sum_{j=1}^B p_{i,j}^{i2t} \log\left(\frac{p_{i,j}^{i2t}}{q_{i,j}^{i2t} + \epsilon}\right), \quad (4)$$

where ϵ is a small constant added to prevent numerical instability. And $q_{i,j}^{i2t} = y_{i,j} / \sum_{k=1}^B y_{i,k}$ represents the true matching probability. Symmetrically, the DTS loss from text to image, \mathcal{L}_{t2i} , mirrors this by exchanging the roles of image and text features. And the bi-directional DTS loss is denoted as:

$$\mathcal{L}_{dts} = \mathcal{L}_{i2t} + \mathcal{L}_{t2i}. \quad (5)$$

3.3 Dual Attribute Prompt Learning (DAPL)

3.3.1 Motivation. To enhance the precision of attribute detection within images, we unveil the Dual Attribute Prompt Learning (DAPL) approach. Diverging from the APL [29], DAPL distinctively leverages both positive and negative attribute prompts. This innovation is primarily achieved through the integration of Dual Image-Attribute Contrastive Learning and Sensitive Attributes Prompt Matching Learning, significantly bolstering the detection of a wide array of attributes.

3.3.2 Dual Image-Attribute Contrastive Learning. Dual Image-Attribute Contrastive (DIAC) Learning employs both positive and negative prompts for contrastive learning at the token-level. Specifically, for each image I_i within an image-attribute batch, we compute similarity scores for both types of prompts against \mathbf{F}_I^i , as described in Eq. 4. For instance, the similarity score for a positive prompt is calculated using the following methodology:

$$S_p^{i2a} = p_{i,j}^{i2t}(\mathbf{F}_I^i, \mathbf{F}_{A_p}^j). \quad (6)$$

Similarly, similarity scores S_p^{a2i} , S_n^{i2a} and S_n^{a2i} are computed. Following [29], for positive attribute prompts, the Positive Image-Attribute Contrastive Learning (PIAC) Loss is given by:

$$\mathcal{L}_{piac} = -\frac{1}{2B} \sum_{A_i^p \in \mathcal{A}} (\log S_p^{i2a} + \log S_p^{a2i}) \quad (7)$$

In a parallel manner, the Negative Image-Attribute Contrastive Learning (NIAC) Loss, \mathcal{L}_{niac} , is calculated, leading to the formulation of the Dual Image-Attribute Contrastive Learning (DIAC) Loss as:

$$\mathcal{L}_{diac} = \frac{1}{2} (\mathcal{L}_{piac} - \mathcal{L}_{niac}) \quad (8)$$

3.3.3 Sensitive Image-Attributes Matching Learning. The similarity scores play a pivotal role in determining the attribute probabilities $\mathbf{p}_{i,j}^a$, effectively accommodating both positive and negative attribute prompts. To maintain balanced sensitivity across attributes, we incorporate a dynamic adjustment factor $\gamma_a^i = \frac{\text{Count}(A_p^i)}{\text{Count}(A_n^i)}$. This factor adjusts the weighting between positive and negative examples for each attribute A_i , ensuring an equitable evaluation.

The attribute probabilities are calculated as:

$$\mathbf{p}_{i,j}^a = \frac{1}{2} \left(\text{softmax}\left(\gamma_a^i S_p^{i2a} - \frac{1}{\gamma_a^i} S_n^{i2a}\right) + \text{softmax}\left(\gamma_a^i S_p^{a2i} - \frac{1}{\gamma_a^i} S_n^{a2i}\right) \right) \quad (9)$$

To refine the matching of sensitive attributes, we employ a specific loss function:

$$\mathcal{L}_{siam} = -\frac{1}{B} \sum_{A_i \in \mathcal{A}} \sum_{j=1}^B \left(y_{i,j} \log(\mathbf{p}_{i,j}^a) + (1 - y_{i,j}) \log(1 - \mathbf{p}_{i,j}^a) \right) \quad (10)$$

3.3.4 Masked Positive Attribute Language Modeling. Masked Attribute Language Modeling (MAM) [29] is designed to predict masked words utilizing clues from matched pairs of images and attribute prompts. Our implementation incorporates the Implicit Relation Reasoning Loss function [13] to refine the prediction of masked attributes. Specifically, we only focus on using masked positive attribute prompts, and the loss function is represented as \mathcal{L}_{mapm} .

To calculate the overall performance of the Dual Attribute Prediction and Learning (DAPL) model, we integrate the contributions from various individual loss functions in a balanced manner:

$$\mathcal{L}_{dapl} = \frac{1}{3} (\mathcal{L}_{diac} + \mathcal{L}_{siam} + \mathcal{L}_{mapm}) \quad (11)$$

3.4 Overall Loss Function

The overall loss function for training our proposed method is defined as:

$$\mathcal{L} = \lambda_{dts} \mathcal{L}_{dts} + \lambda_{mlm} \mathcal{L}_{mlm} + \lambda_{id} \mathcal{L}_{id} + \lambda_{dapl} \mathcal{L}_{DAPL}, \quad (12)$$

where \mathcal{L}_{id} represents the Identity Loss [33], and \mathcal{L}_{mlm} denotes the Implicit Relation Reasoning Loss [13] that utilizes masked text as input. The coefficients λ_{dts} , λ_{mlm} , λ_{id} , and λ_{dapl} are hyperparameters designed to balance the contributions of each component loss to the overall loss function.

4 EXPERIMENTS

4.1 Experimental Setup

4.1.1 Datasets. We evaluate our method on three text-based person retrieval datasets: (1) **CUHK-PEDES** [17] with 34,054 images and 68,108 descriptions for training, plus validation and test sets each with over 3,000 images and 6,000 descriptions, covering 1,000 identities. (2) **ICFG-PEDES** [7], featuring 34,674 image-text pairs for training across 3,102 identities, and nearly 20,000 pairs for testing with descriptions averaging 37 words from a 5,554-word vocabulary. (3) **RSTPReid** [34] offers comprehensive coverage with 5 images and 2 descriptions per identity, segmented into sets with 3,701, 200, and 200 identities, respectively.

Table 1: Performance (%) comparisons with SOTA methods on CUHK-PEDES. Results are ordered based on the Rank-1 accuracy. In the "Type" column, "G" and "L" represent global matching and local matching methods, respectively. "-" indicates that the original paper did not use that specific metric to evaluate its models.

Method	Type	Ref	Image Enc.	Text Enc.	Rank-1	Rank-5	Rank-10	mAP	mINP
DSSL [34]	L	MM21	RN50	BERT	59.98	80.41	87.56	-	-
SSAN [7]	L	arXiv21	RN50	LSTM	61.37	80.15	86.73	-	-
LBUL [26]	L	MM22	RN50	BERT	64.04	82.66	87.22	-	-
Han et al. [10]	G	BMVC21	CLIP-RN101	CLIP-Xformer	64.08	81.73	88.19	60.08	-
CAIBC [25]	L	MM22	RN50	BERT	64.43	82.87	88.37	-	-
AXM-Net [8]	L	MM22	RN50	BERT	64.44	80.52	86.77	58.73	-
IVT [23]	G	ECCVW22	ViT-Base	BERT	65.59	83.11	89.21	-	-
BEAT [19]	L	MM23	RN101	BERT	65.61	83.45	89.57	-	-
CFine [28]	L	arXiv22	CLIP-ViT	BERT	69.57	85.93	91.15	-	-
IRRA [13]	G	CVPR23	CLIP-ViT	CLIP-Xformer	73.38	89.93	93.71	66.13	50.24
BiLMa [9]	G	ICCVW23	CLIP-ViT	CLIP-Xformer	74.03	89.59	93.62	66.57	-
DECL [18]	G	MM23	CLIP-ViT	CLIP-Xformer	75.02	90.89	94.52	-	-
RaSa [1]	G	IJCAI23	ALBEF-ViT	ALBEF-BERT	76.51	90.29	94.25	69.38	-
APTM [29]	L	MM23	ALBEF-ViT	ALBEF-BERT	76.53	90.04	94.15	66.91	-
DualFocus (Ours)	L	-	CLIP-ViT	CLIP-Xformer	77.43	90.73	94.20	68.35	53.56

4.1.2 Evaluation Metrics. TPR (Text-based Person Retrieval) system effectiveness is gauged using the Rank-k metric (common k values: 1, 5, 10), which assesses the likelihood of a correct match in the top- k results of a text query. Additionally, mean average precision (mAP) and mean Inverse Negative Penalty (mINP) [31] are crucial for comprehensive evaluation, reflecting accuracy and relevance for various queries. mAP quantifies the precision of relevant image retrievals, and mINP averages the inverse penalties for relevant pairs, with higher scores in these metrics indicating better performance.

4.1.3 Implementation Details. We adopt the CLIP-ViT-B/16 model as our pre-trained image encoder and the CLIP text transformer as our text encoder [20]. Additionally, we integrate a cross encoder as proposed by [13]. Following [13, 18], we input images are initially resized to 384×128 pixels and undergo a series of augmentations, including random horizontal flipping, random cropping with padding, random erasing, and normalization to enhance the robustness of the model. The maximum token sequence length, n_t , is configured to 77. For optimization, the Adam algorithm [14] is employed over 50 epochs, starting with a learning rate of 1×10^{-5} , and incorporating cosine decay to adjust the learning rate over time. The first 5 epochs serve as a warm-up period, during which the learning rate linearly increases from 1×10^{-6} to 1×10^{-5} . For modules initialized without pre-trained weights, the learning rate is set at 5×10^{-5} from the outset. In our (DTS) loss calculation, we set the temperature parameter τ to 0.02. The regularization parameters λ_{dts} and λ_{dapl} parameters adjusted to 2 and 0.8, respectively. The parameters λ_{mlm} and λ_{id} are both configured with a value of 1. Our models are implemented using PyTorch [12] and trained on 4 NVIDIA RTX 4090 24G GPUs.

4.2 Comparison with State-of-the-Arts

4.2.1 Performance Comparisons on CUHK-PEDES. As illustrated in Table 1, our DualFocus method outperforms a range of state-of-the-art (SOTA) techniques, particularly in Rank-1 accuracy where

it achieves 77.43%, and mean Average Precision (mAP) at 68.35%. These figures signify a substantial leap forward in retrieval accuracy, showcasing DualFocus's adeptness at matching intricate person descriptions with corresponding images. This is largely attributed to its local matching capability, stemming from a detailed image-text alignment strategy. Notably, unlike APTM [29], DualFocus was not pre-trained on the text-to-person synthetic dataset MALS, emphasizing its inherent efficiency. Beyond achieving high Rank-1 accuracy, DualFocus excels across a spectrum of metrics, marked by a remarkable mean Inverse Negative Penalty (mINP) of 53.56. This extensive performance is a testament to DualFocus's prowess in person description retrieval, marking a notable milestone in the domain.

Table 2: Performance (%) comparisons with SOTA methods on ICFG-PEDES dataset.

Method	Type	Rank-1	Rank-5	Rank-10	mAP	mINP
Dual Path [33]	G	38.99	59.44	68.41	-	-
ViTAA [24]	L	50.98	68.79	75.78	-	-
SSAN [7]	L	54.23	72.63	79.53	-	-
IVT [23]	G	56.04	73.60	80.22	-	-
BEAT [19]	L	58.52	75.92	81.96	-	-
CFine [28]	L	60.83	76.55	82.42	-	-
IRRA [13]	G	63.46	80.25	85.82	38.06	7.93
BEAT [19]	L	58.25	75.92	81.96	-	-
BiLMa [9]	G	63.83	80.15	85.74	38.26	-
DECL [18]	G	64.88	81.34	86.72	-	-
RaSa [1]	G	65.28	80.40	85.12	41.29	-
APTM [29]	L	68.51	82.09	87.56	41.22	-
DualFocus (Ours)	L	67.87	81.93	87.13	40.13	9.14

4.2.2 Performance Comparisons on ICFG-PEDES. As shown in Table 2, despite strong performance across several datasets, DualFocus achieves a slightly lower than expected Rank-1 accuracy of 67.87% on the ICFG-PEDES dataset. This figure is slightly below

the leading APTM [29] method, which records a Rank-1 accuracy of 68.51%, prompting a deeper analysis of the dataset’s unique challenges. However, DualFocus still performs well in Rank-5 and Rank-10 accuracy metrics and achieves a significant mINP of 9.14%, demonstrating its robustness in retrieving relevant queries from a large pool. A key feature of the ICFG-PEDES dataset is its privacy-preserving anonymization of faces, which removes crucial semantic details vital for accurate person identification. This reduction significantly affects DualFocus’s performance, underscoring the importance of facial and accessory cues in retrieval tasks. The impact of this anonymization reveals the limitations of current models, including DualFocus, in handling datasets where key identifying features are obscured, highlighting areas for future improvement in model adaptability.

Table 3: Performance (%) comparisons with SOTA methods on RSTPReid dataset.

Method	Type	Rank-1	Rank-5	Rank-10	mAP	mINP
DSSL [34]	G	39.05	62.60	73.95	-	-
SSAN [7]	L	43.50	67.80	77.15	-	-
LBUL [26]	L	45.55	68.20	77.85	-	-
IVT [23]	G	46.70	70.00	78.80	-	-
CFine [28]	L	50.55	72.50	81.60	-	-
IRRA [13]	G	60.20	81.30	88.20	47.17	25.28
RaSa [1]	G	66.90	86.50	91.35	52.31	-
DECL [18]	G	61.35	83.95	90.45	-	-
BEAT [19]	L	48.10	73.10	81.30	-	-
BILMa [9]	G	61.20	81.50	88.80	48.51	-
DECL [18]	G	66.90	86.50	91.35	52.31	-
APTMs [29]	L	67.50	85.70	91.45	52.56	-
DualFocus (Ours)	L	69.12	86.68	92.31	52.55	27.87

4.2.3 Performance Comparisons on RSTPReid. Results in Table 3 highlight DualFocus’s effectiveness on the RSTPReid dataset, achieving a Rank-1 accuracy of 69.12%, outperforming the APTM method. It also excels in Rank-5 and Rank-10 accuracies at 86.68% and 92.31%, respectively, and records a competitive mAP of 52.55% along with the highest mINP of 27.87%, confirming its consistent retrieval quality.

This performance demonstrates DualFocus’s ability to handle the complexities of the RSTPReid dataset, utilizing CLIP-based visual-textual integrations to effectively recognize and differentiate individuals against variable backgrounds and orientations.

Overall, DualFocus consistently delivers excellent results across all benchmark datasets, proving the robustness and generalizability of our method.

4.3 Hyperparameters Analysis

4.3.1 The impact of the λ_{dts} . As shown in Figure 3, setting $\lambda_{dts} = 2$ in our analysis of the CUHK-PEDES dataset achieves the highest Rank-1 accuracy. This optimal value indicates that the Dynamic Tokenwise Similarity (DTS) loss effectively balances the model’s focus between global features and localized, part-based features. This balance is crucial as it allows the model to accurately compute token-wise similarities, aligning detailed visual cues with textual descriptors at a granular level. This precision is key in person re-identification tasks, where subtle visual differences significantly

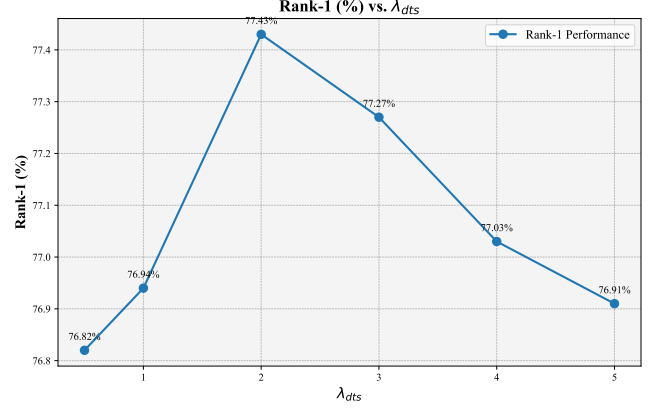


Figure 3: The impact of λ_{dts} on R@1 on CUHK-PEDES.

impact the matching accuracy of person images with their corresponding descriptions.

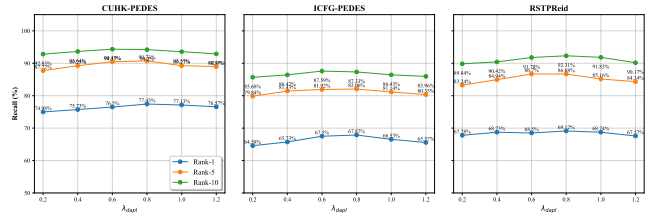


Figure 4: The impact of λ_{dpal} on R@1,5,10 on CUHK-PEDES, ICFG-PEDES, and RSTPReid.

4.3.2 The impact of the λ_{dpal} . As shown in Figure 4, optimizing λ_{dpal} to 0.8 markedly improves person re-identification accuracies (Rank-1, Rank-5, and Rank-10), demonstrating the effectiveness of dual attribute prompt learning in refining attribute recognition. This adjustment enhances the model’s ability to discern nuanced attributes, thereby improving precision across diverse scenarios.

The impact of λ_{dpal} across datasets highlights its crucial role in adapting to complex real-world conditions, boosting the model’s versatility and robustness. Fine-tuning λ_{dpal} along with λ_{dts} is essential for enhancing the performance of advanced recognition models, leading to better accuracy and adaptability in person re-identification tasks.

4.4 Ablation Study

4.4.1 Effectiveness of the Dynamic Tokenwise Similarity (DTS) Loss. Incorporating the Dynamic Tokenwise Similarity (DTS) loss function into the baseline model, identified as IRRA, results in significant improvements in Rank-1 accuracy across all datasets. The model’s performance increases to 74.09% on CUHK-PEDES, 65.24% on ICFG-PEDES, and 65.73% on RSTPReid. This improvement underscores the DTS loss’s capability in dynamically selecting challenging samples, thereby enhancing the model’s discriminative power and fine-grained matching precision over the Static Discriminative Margin (SDM) loss [13].

Table 4: Ablation experimental results (%) on the effectiveness of each component in DualFocus. The "Baseline" represents the IRRA [13] model.

No.	Methods	Components			CUHK-PEDES			ICFG-PEDES			RSTPReid		
		\mathcal{L}_{dts}	\mathcal{L}_{diac}	\mathcal{L}_{siam}	Rank-1	Rank-5	Rank-10	Rank-1	Rank-5	Rank-10	Rank-1	Rank-5	Rank-10
1	Baseline				73.38	89.93	93.71	63.46	80.25	85.82	60.20	81.30	88.20
2	+ \mathcal{L}_{dts}	✓			74.09	90.85	93.89	65.24	80.63	86.01	65.73	75.32	87.28
3	+ \mathcal{L}_{diac}		✓		73.77	89.72	92.98	62.56	79.35	84.71	59.24	82.26	87.55
4	+ \mathcal{L}_{siam}			✓	74.13	88.81	93.31	64.92	81.04	85.18	68.27	82.90	86.59
5	+DAPL		✓	✓	75.20	89.32	93.81	66.76	81.31	85.68	67.07	83.11	86.98
6	DualFocus	✓	✓	✓	77.43	90.73	94.20	67.87	82.06	87.33	69.12	86.68	92.31

Table 5: Performance (%) comparisons of SOTA (State-of-the-Art) Methods with Negative Descriptors on the CUHK-PEDES, ICFG-PEDES, and RSTPReid Datasets.

Methods	CUHK-PEDES				ICFG-PEDES				RSTPReid			
	Rank-1	Rank-5	Rank-10	mAP	Rank-1	Rank-5	Rank-10	mAP	Rank-1	Rank-5	Rank-10	mAP
IRRA [13]	76.82	82.63	93.88	67.89	67.04	84.28	87.66	38.83	65.88	82.29	93.88	50.28
DECL [18]	77.06	84.27	94.16	68.43	68.73	84.42	88.58	39.42	64.16	84.45	92.01	53.81
RaSa [1]	78.64	85.42	94.67	69.28	69.27	84.35	89.44	40.21	67.17	85.45	91.19	54.97
DualFocus	80.05	87.65	96.48	70.02	70.42	84.68	89.59	41.37	69.84	87.96	94.62	56.98

4.4.2 Effectiveness of Dual Attribute Prompts Learning (DAPL). The DAPL component, which synergistically combines \mathcal{L}_{diac} and \mathcal{L}_{siam} , further elevates the model’s performance. \mathcal{L}_{diac} maintains consistency across different representations of similar entities, whereas \mathcal{L}_{siam} focuses on refining the model’s sensitivity to variable data interactions, thereby reducing intra-class variations. Independently, each contributes significantly; however, their integration under DAPL leads to enhanced model performance with Rank-1 accuracies rising to 75.20% on CUHK-PEDES, 66.76% on ICFG-PEDES, and 67.07% on RSTPReid. These results highlight DAPL’s crucial role in balancing input data aspects during training and refining the model’s focus, thereby improving its understanding of complex visual-textual relationships.

4.4.3 Combined Effectiveness of DTS and DAPL. The integration of both DTS and DAPL within the DualFocus configuration achieves the highest performance metrics across all evaluated datasets, indicating the synergistic effect of these components. This potent combination attains Rank-1 accuracies of 77.43% on CUHK-PEDES, 67.87% on ICFG-PEDES, and 69.12% on RSTPReid. The combined implementation not only reinforces the model’s discriminative power but also significantly enhances its ability to accurately match textual descriptions with corresponding images, thereby setting a new benchmark in person description retrieval tasks.

4.4.4 Summary. The ablation study clearly demonstrates that both the DTS and DAPL components are integral to the DualFocus framework, significantly contributing to its enhanced performance. The

study also reveals that while each component independently improves the model’s accuracy, their integration yields the most substantial performance gains, thereby validating the proposed framework’s effectiveness in leveraging complex visual-textual interplays for person description retrieval.

4.5 Analysis of Sensitivity to Negative Descriptors

In this section, we evaluated the robustness of our DualFocus model against negative descriptors in textual queries. We augmented the textual queries by introducing two negative descriptors, derived from the predefined attribute table [29], to assess the models’ ability to effectively exclude irrelevant information.

The empirical results, outlined in Table 5, show that DualFocus consistently outperforms competing methods in both Rank-1 accuracy and mean Average Precision (mAP) across all datasets. Specifically, DualFocus achieved Rank-1 accuracies of 80.05%, 70.42%, and 69.84% on each respective dataset. These results highlight the model’s ability to maintain high precision and accuracy by effectively managing misleading descriptors.

The integration of two negative descriptors from a predefined attribute table rigorously tests the models’ ability to discern relevant from non-relevant features. DualFocus’s superior performance is enabled by its innovative architecture that combines Dynamic Tokenwise Similarity (DTS) and Dual Attribute Prompt Learning (DAPL), enhancing its handling of complex visual-textual interactions. This makes DualFocus highly effective in scenarios with imprecise or incorrect textual queries, maintaining high accuracy despite potential distractions.

4.6 Comparisons on the domain generalization task

Table 6: Cross-Domain performance (%) between CUHK-PEDES and ICFG-PEDES. Here “C” denotes CUHK-PEDES, while “I” represents ICFG-PEDES.

Method	C → I			I → C		
	R@1	R@5	R@10	R@1	R@5	R@10
SSAN [7]	29.24	49.00	58.53	21.07	38.94	48.54
IRRA [13]	41.67	61.06	69.24	30.36	52.86	65.51
DCEL [18]	43.31	62.29	70.31	32.35	54.86	65.51
DualFocus	50.47	68.62	74.60	45.34	62.67	75.43

We conducted a rigorous evaluation of our DualFocus framework on the CUHK-PEDES and ICFG-PEDES datasets to assess its domain generalization capabilities. The results, detailed in Table 6, show that DualFocus substantially outperforms contemporary models like SSAN [7], IRRA [13], and DCEL [18]. For instance, DualFocus achieved a Rank-1 accuracy of 50.47% when trained on CUHK-PEDES and tested on ICFG-PEDES, notably higher than its competitors. This performance highlights DualFocus’s strength in handling domain variations and its ability to generalize well across different data distributions, owing to its innovative architecture that effectively integrates visual and textual data, enhancing adaptability and robustness in real-world scenarios.

5 CONCLUSION

In this paper, we introduce DualFocus, a novel framework designed to enhance text-based person retrieval (TPR) systems by integrating both positive and negative descriptors. Through the Dual Attribute Prompt Learning (DAPL) and the Dynamic Tokenwise Similarity (DTS) loss, DualFocus achieves precise attribute alignment and fine-grained attribute matching, significantly boosting system performance. This advancement not only improves the accuracy and efficiency of traditional TPR systems but also propels the development of multimodal retrieval technologies, demonstrating the potential of combining linguistic and visual data to tackle complex retrieval challenges. In future work, addressing the generation of negative descriptors remains a crucial challenge for the DualFocus model. Currently, relying on a predefined list of attributes to generate negative examples during training limits the model’s ability to capture the diversity and complexity of natural language descriptions and real-world scenarios. This constraint impacts the diversity and practical applicability of DualFocus.

REFERENCES

- [1] Yang Bai, Min Cao, Daming Gao, Ziqiang Cao, Chen Chen, Zhenfeng Fan, Liqiang Nie, and Min Zhang. 2023. RaSa: relation and sensitivity aware representation learning for text-based person search. In *Proceedings of the Thirty-Second International Joint Conference on Artificial Intelligence*. 555–563.
- [2] Mathilde Caron, Hugo Touvron, Ishan Misra, Hervé Jégou, Julien Mairal, Piotr Bojanowski, and Armand Joulin. 2021. Emerging properties in self-supervised vision transformers. In *Proceedings of the IEEE/CVF international conference on computer vision*. 9650–9660.
- [3] Dapeng Chen, Hongsheng Li, Xihui Liu, Yantao Shen, Jing Shao, Zejian Yuan, and Xiaogang Wang. 2018. Improving deep visual representation for person re-identification by global and local image-language association. In *ECCV*. 54–70.
- [4] Xinlei Chen, Haoqi Fan, Ross Girshick, and Kaiming He. 2020. Improved baselines with momentum contrastive learning. *arXiv preprint arXiv:2003.04297* (2020).
- [5] Yuhao Chen, Guoqing Zhang, Yujiang Lu, Zhenxing Wang, and Yuhui Zheng. 2022. TIPCB: A simple but effective part-based convolutional baseline for text-based person search. *Neurocomputing* 494 (2022), 171–181.
- [6] Wenliang Dai, Junnan Li, Dongxu Li, Anthony Meng Huat Tiong, Junqi Zhao, Weisheng Wang, Boyang Li, Pascale Fung, and Steven Hoi. 2023. InstructBLIP: Towards General-purpose Vision-Language Models with Instruction Tuning. *arXiv:2305.06500* [cs.CV]
- [7] Zefeng Ding, Changxing Ding, Zhiyin Shao, and Dacheng Tao. 2021. Semantically self-aligned network for text-to-image part-aware person re-identification. *arXiv preprint arXiv:2107.12666* (2021).
- [8] Ammarah Farooq, Muhammad Awais, Josef Kittler, and Syed Safwan Khalid. 2022. AXM-Net: Implicit Cross-Modal Feature Alignment for Person Re-identification. In *AAAI*, Vol. 36. 4477–4485.
- [9] Takuro Fujii and Shuhei Tarashima. 2023. BiLMA: Bidirectional Local-Matching for Text-based Person Re-identification. In *Proceedings of the IEEE/CVF International Conference on Computer Vision*. 2786–2790.
- [10] Xiao Han, Sen He, Li Zhang, and Tao Xiang. 2021. Text-based person search with limited data. *arXiv preprint arXiv:2110.10807* (2021).
- [11] Kaiming He, Haoqi Fan, Yuxin Wu, Saining Xie, and Ross Girshick. 2020. Momentum contrast for unsupervised visual representation learning. In *Proceedings of the IEEE/CVF conference on computer vision and pattern recognition*. 9729–9738.
- [12] Sagar Imambi, Kolla Bhanu Prakash, and GR Kanagachidambaresan. 2021. PyTorch. *Programming with TensorFlow: Solution for Edge Computing Applications* (2021), 87–104.
- [13] Ding Jiang and Mang Ye. 2023. Cross-Modal Implicit Relation Reasoning and Aligning for Text-to-Image Person Retrieval. In *Proceedings of the IEEE/CVF Conference on Computer Vision and Pattern Recognition*. 2787–2797.
- [14] Diederik P Kingma and Jimmy Ba. 2015. Adam: A Method for Stochastic Optimization. In *ICLR (Poster)*.
- [15] Junnan Li, Dongxu Li, Silvio Savarese, and Steven Hoi. 2023. Blip-2: Bootstrapping language-image pre-training with frozen image encoders and large language models. *arXiv preprint arXiv:2301.12597* (2023).
- [16] Junnan Li, Ramprasaath Selvaraju, Akhilesh Gotmare, Shafiq Joty, Caiming Xiong, and Steven Chu Hong Hoi. 2021. Align before fuse: Vision and language representation learning with momentum distillation. *Advances in neural information processing systems* 34 (2021), 9694–9705.
- [17] Shuang Li, Tong Xiao, Hongsheng Li, Bolei Zhou, Dayu Yue, and Xiaogang Wang. 2017. Person search with natural language description. In *Proceedings of the IEEE conference on computer vision and pattern recognition*. 1970–1979.
- [18] Shenshen Li, Xing Xu, Yang Yang, Fumin Shen, Yijun Mo, Yujie Li, and Heng Tao Shen. 2023. DCEL: Deep Cross-modal Evidential Learning for Text-Based Person Retrieval. In *Proceedings of the 31st ACM International Conference on Multimedia*. 6292–6300.
- [19] Yiwei Ma, Xiaoshuai Sun, Jiayi Ji, Guannan Jiang, Weilin Zhuang, and Rongrong Ji. 2023. Beat: Bi-directional One-to-Many Embedding Alignment for Text-based Person Retrieval. In *Proceedings of the 31st ACM International Conference on Multimedia*. 4157–4168.
- [20] Alec Radford, Jong Wook Kim, Chris Hallacy, Aditya Ramesh, Gabriel Goh, Sandhini Agarwal, Girish Sastry, Amanda Askell, Pamela Mishkin, Jack Clark, et al. 2021. Learning transferable visual models from natural language supervision. In *International conference on machine learning*. PMLR, 8748–8763.
- [21] Rico Sennrich, Barry Haddow, and Alexandra Birch. 2015. Neural machine translation of rare words with subword units. *arXiv preprint arXiv:1508.07909* (2015).
- [22] Zhiyin Shao, Xinyu Zhang, Meng Fang, Zhifeng Lin, Jian Wang, and Changxing Ding. 2022. Learning granularity-unified representations for text-to-image person re-identification. In *Proceedings of the 30th ACM International Conference on Multimedia*. 5566–5574.
- [23] Xiujun Shu, Wei Wen, Haoqian Wu, Keyu Chen, Yiran Song, Ruizhi Qiao, Bo Ren, and Xiao Wang. 2022. See finer, see more: Implicit modality alignment for text-based person retrieval. In *European Conference on Computer Vision*. Springer, 624–641.
- [24] Zhe Wang, Zhiyuan Fang, Jun Wang, and Yezhou Yang. 2020. Vitaa: Visual-textual attributes alignment in person search by natural language. In *ECCV*. 402–420.
- [25] Zijie Wang, Aichun Zhu, Jingyi Xue, Xili Wan, Chao Liu, Tian Wang, and Yifeng Li. 2022. Caibc: Capturing all-round information beyond color for text-based person retrieval. In *Proceedings of the 30th ACM International Conference on Multimedia*. 5314–5322.
- [26] Zijie Wang, Aichun Zhu, Jingyi Xue, Xili Wan, Chao Liu, Tian Wang, and Yifeng Li. 2022. Look before you leap: Improving text-based person retrieval by learning a consistent cross-modal common manifold. In *Proceedings of the 30th ACM International Conference on Multimedia*. 1984–1992.
- [27] Yushuang Wu, Zizheng Yan, Xiaoguang Han, Guanbin Li, Changqing Zou, and Shuguang Cui. 2021. LapsCore: language-guided person search via color reasoning. In *Proceedings of the IEEE/CVF International Conference on Computer Vision*. 1624–1633.

- [28] Shuanglin Yan, Neng Dong, Liyan Zhang, and Jinhui Tang. 2022. Clip-driven fine-grained text-image person re-identification. *arXiv preprint arXiv:2210.10276* (2022).
- [29] Shuyu Yang, Yinan Zhou, Yaxiong Wang, Yujiao Wu, Li Zhu, and Zhedong Zheng. 2023. Towards Unified Text-based Person Retrieval: A Large-scale Multi-Attribute and Language Search Benchmark. In *Proceedings of the 2023 ACM on Multimedia Conference*.
- [30] Lewei Yao, Runhui Huang, Lu Hou, Guansong Lu, Minzhe Niu, Hang Xu, Xiaodan Liang, Zhenguo Li, Xin Jiang, and Chunjing Xu. 2021. Filip: Fine-grained interactive language-image pre-training. *arXiv preprint arXiv:2111.07783* (2021).
- [31] Mang Ye, Jianbing Shen, Gaojie Lin, Tao Xiang, Ling Shao, and Steven CH Hoi. 2021. Deep learning for person re-identification: A survey and outlook. *IEEE Transactions on Pattern Analysis and Machine Intelligence (TPAMI)* (2021).
- [32] Jiahui Yu, Zirui Wang, Vijay Vasudevan, Legg Yeung, Mojtaba Seyedhosseini, and Yonghui Wu. 2022. Coca: Contrastive captioners are image-text foundation models. *arXiv preprint arXiv:2205.01917* (2022).
- [33] Zhedong Zheng, Liang Zheng, Michael Garrett, Yi Yang, Mingliang Xu, and Yi-Dong Shen. 2020. Dual-path convolutional image-text embeddings with instance loss. *ACM Transactions on Multimedia Computing, Communications, and Applications (TOMM)* 16, 2 (2020), 1–23.
- [34] Aichun Zhu, Zijie Wang, Yifeng Li, Xili Wan, Jing Jin, Tian Wang, Fangqiang Hu, and Gang Hua. 2021. Dssl: Deep surroundings-person separation learning for text-based person retrieval. In *Proceedings of the 29th ACM International Conference on Multimedia*. 209–217.